

# Visualizing Tumors in Real Time: A Highly Sensitive PSMA Probe for NIR-II Imaging and Intraoperative Tumor Resection

Longfei Zhang, Xiaojing Shi, Yuying Li, Xiaojiang Duan, Zeyu Zhang, Hualong Fu, Xing Yang, Jie Tian, Zhenhua Hu,\* and Mengchao Cui\*

Cite This: *J. Med. Chem.* 2021, 64, 7735–7745

Read Online

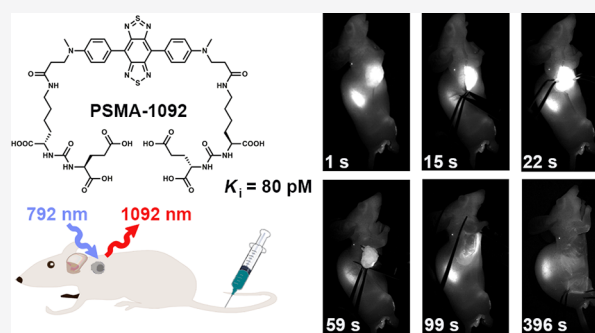
ACCESS |

Metrics & More

Article Recommendations

Supporting Information

**ABSTRACT:** Owing to the complex anatomical structure, precise resection of a tumor while maintaining adjacent tissue is a challenge in radical prostatectomy for prostate cancer (PCa). Optical imaging in near-infrared window II (NIR-II) is a promising technology for intraoperative guidance, whereas there is no available probe for PCa yet. In this article, a novel probe (PSMA-1092) bearing two prostate-specific membrane antigen (PSMA) binding motifs was developed, displaying excellent optical properties ( $\lambda_{\max} = 1092$  nm) and ultrahigh affinity ( $K_i = 80$  pM) toward PSMA. The tumor was visualized with high resolution (tissue-to-normal tissue ratio =  $7.62 \pm 1.05$ ) and clear margin by NIR-II imaging using PSMA-1092 in a mouse model. During the tumor resection, residual tumors missed by visible inspection were detected by the real-time imaging. Overall, PSMA-1092 displayed excellent performance in delineating the tumor margin and detecting residual tumors, demonstrating promising potential for precise PCa tumor resection in clinical practice.



## INTRODUCTION

In the past decades, the incidence rates of prostate cancer (PCa) have increased rapidly worldwide, and it has become one of the leading causes of tumor-related deaths in males.<sup>1,2</sup> Even though several drugs for treating PCa have been developed,<sup>3–5</sup> radical prostatectomy is still the most effective treatment and first choice for patients in early stages.<sup>6,7</sup> Owing to the irregular and indistinctive tumor boundary, a positive surgical margin in radical prostatectomy specimens is a common issue,<sup>8</sup> which may increase the risk of recurrence and metastasis<sup>9–12</sup> and thus deteriorate the prognoses of patients.<sup>13</sup> Moreover, excessive resection could easily injure the abundant nerves and vessels in this region, which could lead to various complications, such as urinary incontinence and urethrostenosis.<sup>14,15</sup> Therefore, developing a novel imaging technology for aiding surgeons to precisely delineate tumor margins and detect missed lesions during surgery in real time with high resolution is highly desirable and demanded.

Compared to the traditional imaging modalities, such as computed tomography and magnetic resonance imaging, optical imaging in the near-infrared window I (NIR-I, 650–900 nm) has been demonstrated to have many advantages, for example, being easy to implement, providing fast signal feedback, and showing no exposure to radiation.<sup>16–19</sup> According to recent studies, the imaging quality can be dramatically improved by detecting in the near-infrared window II (NIR-II, 1000–1700 nm) because of a lower level of tissue autofluorescence, minimal photon scattering and photoabsorption, which leads to a deeper

penetration capacity, high spatial and temporal resolution, and powerful sensitivity.<sup>20–24</sup> Based on the above advantages, optical imaging in the NIR-II window is highly suitable for intraoperative fluorescent imaging guidance of precise tumor resection.<sup>25–28</sup>

After the report of the first small organic NIR-II fluorescent probe in 2016,<sup>29</sup> great efforts have been devoted to develop probes and technologies for NIR-II imaging.<sup>30–34</sup> In 2019, Tian's group developed a novel multispectral imaging instrument, which could detect an optical signal in both NIR-I and NIR-II regions, and successfully implemented it into the precise tumor resection of patients with liver cancer in clinical practice.<sup>35</sup> Even though the novel imaging instrument demonstrated good performance and successfully detected an extrahepatic metastasis missed by the surgeon in one case, it still suffered from some limitations, such as false positives, owing to the lack of appropriate NIR-II agent. Hence, the development of new NIR-II agents with excellent optical and biological properties could effectively facilitate the clinical translation of NIR-II imaging.

Received: March 11, 2021

Published: May 28, 2021



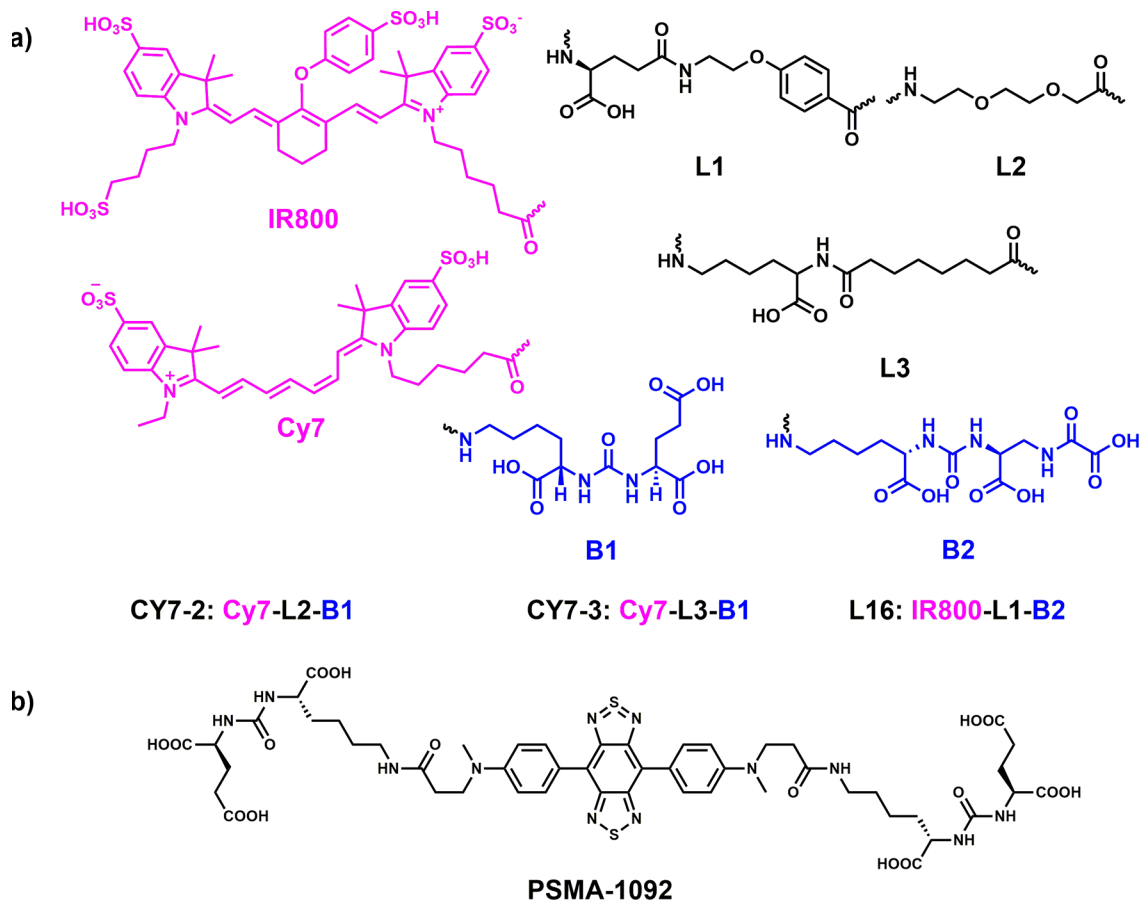


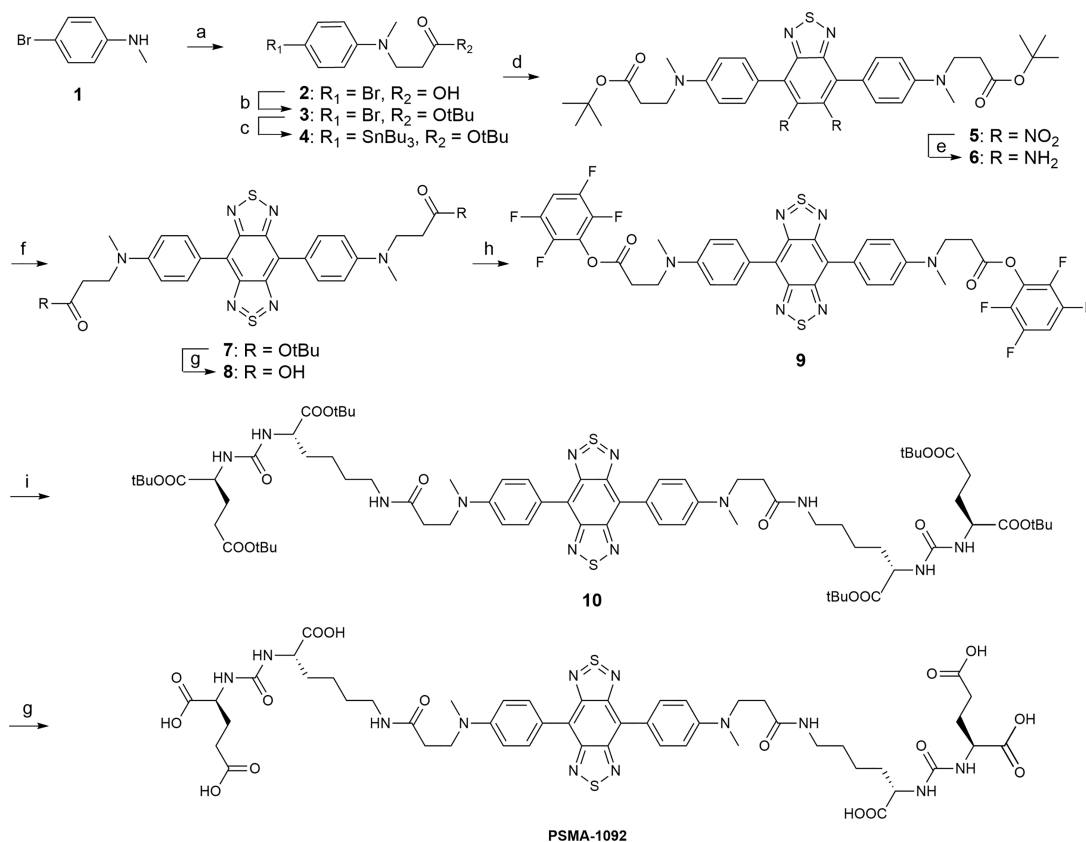
**Figure 1.** (a) Structures of previously reported fluorescent PSMA probes. Blue indicates the binding motif, and purple indicates the fluorescent fluorophores in the NIR-I region. (b) Structure of the newly designed NIR-II PSMA probe.

In recent years, diverse NIR-II probes based on single-walled carbon nanotubes, quantum dots, and rare-earth-doped nanoparticles have been developed and have demonstrated excellent optical properties.<sup>36–38</sup> However, owing to the long-term retention in the reticuloendothelial system and the lack of long-term safety study, it is almost impossible for these probes to be applied in clinical practice.<sup>38,39</sup> Oppositely, because of the excellent biocompatibility and quick clearance capacity through the metabolic system, the molecular probe is considered as a promising candidate for biological imaging and attracts intense focus. Even though some NIR-II organic molecular probes were developed in recent years, the majority of them encounter bottlenecks because of the lack of a definite target and poor water solubility, which are an inevitable obstruction to clinical transformation. Therefore, developing a novel NIR-II organic molecular probe with high water solubility and certain targeting site is urgent to address this dilemma.

Prostate-specific membrane antigen (PSMA) is a type II transmembrane glycoprotein which is overexpressed on the cell membrane of primary and metastatic prostate tumors, and the PSMA expression level positively correlates to the stages of PCa and Gleason score.<sup>9,40,41</sup> As a result, PSMA attracts intense attention as an effective biomarker for assessing PCa, and several probes targeting it for optical imaging have been developed in recent years (Figure 1a).<sup>12,42–46</sup> In 2012, Pomper's group designed a series of fluorescent PSMA probes with different linkers based on commercial fluorophores to explore the relationship between linker length and affinities.<sup>47</sup> Among these probes, compounds CY7-2 and CY7-3, with long linkers,

displayed high affinities ( $K_i = 7$  pM for CY7-2 and 5 pM for CY7-3) to PSMA and excellent performance with *in vivo* imaging. More recently, an IRDye800CW-based probe, L16, was reported by Yang's group, which demonstrated impressive biological properties ( $K_i = 0.65$  nM) and successfully visualized the tumor in a mouse model at 4 h postinjection.<sup>48</sup> A further *ex vivo* biodistribution study indicated that the tumor-to-muscle ratio could reach 19.0 at 24 h postinjection. However, these probes suffer from the inherent drawbacks of NIR-I probes, such as poor tissue-penetrating capability and limited resolution because of their short fluorescence emission wavelengths (emission maxima of CY7-3, CY7-2, and L16 in phosphate-buffered saline (PBS) are 767, 767, and 800 nm, respectively).

In this study, a novel small organic NIR-II fluorescent probe was designed with favorable optical properties, super water solubility, and clinical transformation potential to provide efficient fluorescent guidance in prostate tumor resection. Considering that the donor–acceptor–donor (D–A–D) core structure and appropriate electron acceptor and electron donor moieties are the key factors to obtain NIR-II fluorescent probes,<sup>49,50</sup> the benzobis(1,2,5-thiadiazole) moiety was selected as an excellent electron acceptor<sup>36,37</sup> and conjugated two *N*-methylaniline as electron donors. More importantly, two (((*S*)-5-amino-1-carboxypentyl)carbamoyl)-*L*-glutamic acid (Glu-urea-Lys) moieties as specific binding moieties toward PSMA were incorporated into the *N*-methylamino group via a short amide linker to enhance the binding affinity (Figure 1b). In addition to the prominent binding ability, the three carboxy groups on Glu-urea-Lys moieties could endow the probe with

Scheme 1. Synthetic Route of PSMA-1092<sup>a</sup>

<sup>a</sup>Reagents and conditions: (a) acrylic acid, acetic acid (20% in H<sub>2</sub>O), 100 °C, overnight, 94.5%; (b) *tert*-butanol, DCC, DMAP, CH<sub>2</sub>Cl<sub>2</sub>, room temperature, overnight, 43.2%; (c) hexabutyl-distannane, Pd(PPh<sub>3</sub>)<sub>4</sub>, toluene, N<sub>2</sub>, 120 °C, 2 h; (d) 4,7-dibromo-5,6-dinitrobenzo[*c*][1,2,5]-thiadiazole, PdCl<sub>2</sub>(PPh<sub>3</sub>)<sub>2</sub>, toluene, N<sub>2</sub>, 120 °C, 2 h, 7.7%; (e) iron powder, acetic acid, 100 °C, 30 min, 36.2%; (f) PhNSO, TMSCl, dry pyridine, 80 °C, overnight, 27.2%; (g) TFA, CH<sub>2</sub>Cl<sub>2</sub>, room temperature, 4 h, 100%; (h) 2,3,5,6-tetrafluorophenol, DCC, CH<sub>2</sub>Cl<sub>2</sub>, room temperature, 5 h, 67.4%; (i) di-*tert*-butyl (((*S*)-6-amino-1-(*tert*-butoxy)-1-oxohexan-2-yl)carbamoyl)-*L*-glutamate, Et<sub>3</sub>N, CH<sub>2</sub>Cl<sub>2</sub>, room temperature, 6 h, 61.3%.

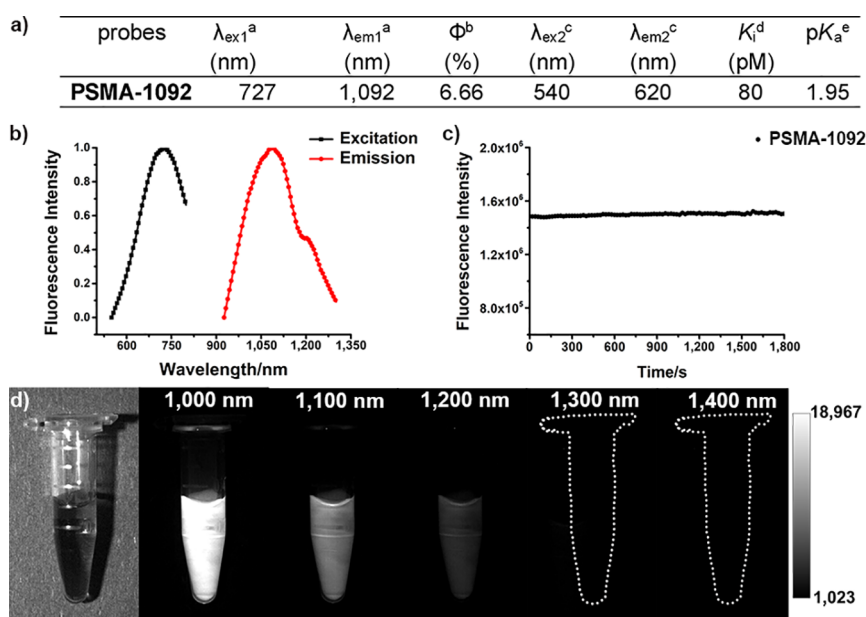


**Figure 2.** (a) Optical properties table of PSMA-1092. <sup>a</sup>Absorption ( $\lambda_{ex1}$ ) and emission ( $\lambda_{em1}$ ) maximum recorded in DMSO. <sup>b</sup>Quantum yield measured in PBS. <sup>c</sup>Absorption ( $\lambda_{ex2}$ ) and emission ( $\lambda_{em2}$ ) spectra determined in acid aqueous solution (pH 2.66). <sup>d</sup> $K_i$  value measured by the inhibition assay using the lysate of LNCaP cell. <sup>e</sup>The  $pK_a$  value was calculated based on the Boltzmann curve. (b) UV-vis-NIR absorption and fluorescence emission spectra of PSMA-1092 (10  $\mu$ M) in DMSO. (c) Photostability of PSMA-1092 (10  $\mu$ M) in DMSO under 727 nm continuous laser exposure. (d) NIR-II imaging of PSMA-1092 (0.43 mM) in PBS with various LP filters. White dotted line contours the invisible solution.

high hydrophilicity, which could significantly improve its solubility in aqueous solution.

## RESULTS AND DISCUSSION

**Synthesis.** The synthetic route of PSMA-1092 is shown in Scheme 1. Acrylic acid as a functional linker was reacted with 4-bromo-*N*-methylaniline in aqueous acetic acid to provide compound 2 with a high yield (94.5%). The carboxy group was then protected with *tert*-butanol, which was stable in subsequent reactions. After the bromine atom was replaced with a tributyltin group, a Stille cross-coupling reaction was performed between the tributyltin derivative and the commercially available 4,7-dibromo-5,6-dinitrobenzo[*c*][1,2,5]-thiadiazole in methylbenzene to provide compound 5 with moderate yield (17.7%). Then nitro reduction and *N*-thionylaniline-induced cyclization were used in sequence to build the core structure of the NIR-II fluorophore (36.2 and 37.5% yield, respectively). After the *tert*-butanol groups in compound 7 were removed by a TFA/DCM system, the carboxy derivative was reacted with 2,3,5,6-tetrafluorophenol to produce the active ester (compound 9) with a high yield (67.4%). Then two *tert*-butanol-protected Glu-urea-Lys binding moieties were conjugated with the NIR-II fluorophore via an amide bond to give compound 10 (61.3% yield). The final product, PSMA-1092, was obtained as a dark green crystal in high yield (98.4%) after the deprotection of all *tert*-butyl groups. All intermediates were characterized by <sup>1</sup>H NMR and MS, and PSMA-1092 was characterized by <sup>1</sup>H NMR, <sup>13</sup>C NMR, and HRMS. The purity of PSMA-1092 was determined as 97.3% using high-performance liquid chromatography (HPLC, Figure S1).

**Optical Properties.** Owing to the intense intramolecular charge transfer (ICT) effect in the D–A–D structure, the fluorescence emission peak of PSMA-1092 was measured at 1092 nm (DMSO, Figure 2a,b and Figures S2a–d and S4), which was in the NIR-II region and similar to other probes based on the benzobis(1,2,5-thiadiazole) fluorophore.<sup>20,36,39</sup> Moreover, the probe demonstrated a large Stokes shift (365 nm, DMSO, Figure 2a,b) compared to that in previously reported NIR-II probes,<sup>36</sup> which could decrease the self-quenching of the imaging agent and avoid the influence of an excitation laser, consequently leading to improved image quality in NIR-II imaging. To verify the photostability of PSMA-1092, its DMSO solution was exposed to 30 min continuous radiation under an excitation laser (727 nm, 10 W). During the above process, no obvious photodegradation was observed (Figure 2c), indicating its outstanding light stability. The quantum yield of PSMA-1092 was measured as 6.66% in PBS, which is high enough for NIR-II imaging and is expected to have a good performance in further investigation. The NIR-II fluorescence signal of PSMA-1092 in PBS was further compared under various long-pass (LP) filters using an NIR-II imaging system. The PSMA-1092 solution was visualized under 1000–1200 nm LP filters, whereas no signal was detected with a 1300 or 1400 nm filter (Figure 2d). Considering that the fluorescence signal under a 1000 nm LP filter was stronger than others, it was selected for further in vivo NIR-II imaging. To investigate the penetration ability of PSMA-1092, the NIR-II images of its aqueous solution (0.5 mg/mL, with 5% DMSO, filled in a capillary glass tube in advance) under different thicknesses of chicken breast tissues were acquired. An intense fluorescence signal of PSMA-1092 could be observed under 2.98 mm of chicken breast tissue, and the signal could still be detected when 3.72 mm of cover tissue was used (Figure S2e), guaranteeing the sensitivity of our probe during surgery. In

general, the probes possess a favorable fluorescence emission wavelength, a large Stokes shift, and excellent photostability property, showing great potential for in vivo NIR-II imaging.

Interestingly, the fluorescence property of PSMA-1092 demonstrated a dramatic change in solutions with different pH values (Figure 3a,b), which could be observed by the naked eyes (Figure 3c). After being exposed to an acid solution, the color of the PSMA-1092 solution changed to bright pink from cyan under natural light, and a gradually increasing fluorescence could be observed under 365 nm ultraviolet light (Figure 3d) or in NIR-I imaging (Figure 3e). Fluorescence spectra indicated that the fluorescence maxima shifted to 620 nm from 1092 nm in

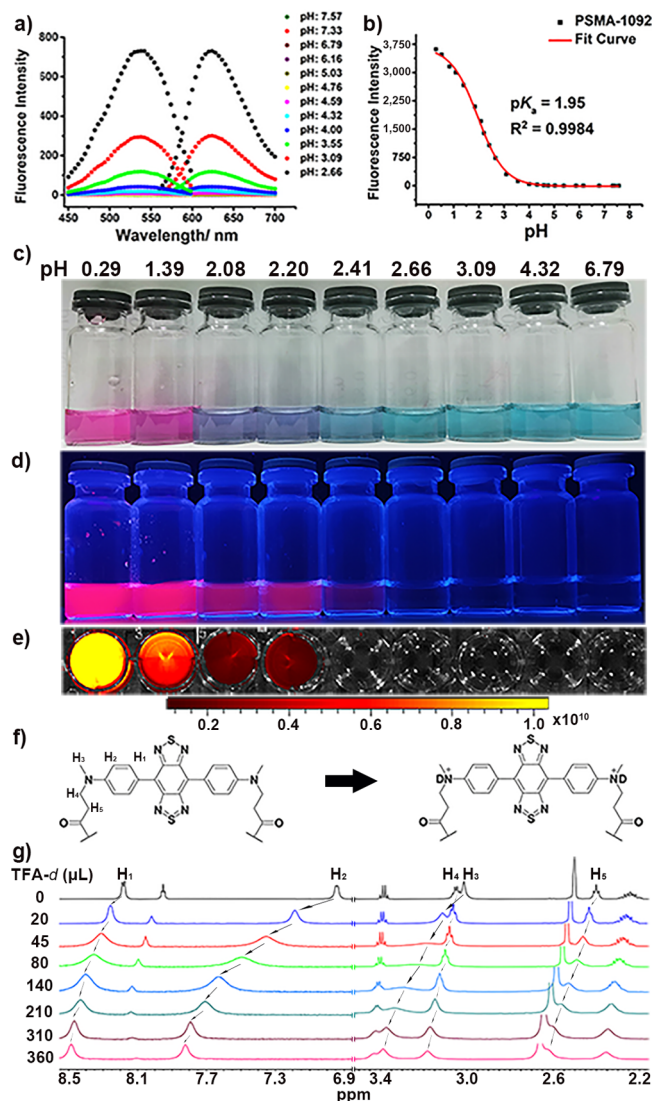


**Figure 3.** (a) UV–vis–NIR absorption spectra and fluorescence emission spectra of PSMA-1092 in aqueous solution with different pH values. (b) Plots of the fluorescence (0.1 mM) signal intensities at 620 nm versus the pH values for PSMA-1092 within the range of 0–7.5. The  $pK_a$  values were calculated to be 1.95 based on the Boltzmann fitting method, and the  $R^2$  was measured as 0.9984. (c,d) Photograph of PSMA-1092 aqueous solution with different pH under natural light (c) and 365 nm ultraviolet light (d). (e) NIR-I imaging of the above solutions. (f) Possible protonation mechanism of PSMA-1092 in an acid environment. (g) <sup>1</sup>H NMR spectra (600 MHz, DMSO-*d*<sub>6</sub>) of PSMA-1092 upon different amounts of deuterated TFA in 1.5 mL of DMSO-*d*<sub>6</sub>. Arrows indicate the peaks with shifts.

acid conditions, and the fluorescence intensity at 620 nm was greatly improved with the increasing acidity of the solution (Figure 3a,b). When the pH of the solution changed from 7 to 0.3, the fluorescence intensity of PSMA-1092 increased by 85 times. Further quantitative analysis reveals that the signal intensity of the new fluorescence maximum is linearly correlated with the concentration of  $H^+$  within a limited pH range (pH 1–2, Figure S3). In addition, plots of fluorescence intensities of PSMA-1092 at 620 nm and the pH values are well fitted by the Boltzmann curve ( $R^2 = 0.9984$ ), and the  $pK_a$  value is calculated to be 1.95 (Figure 3b). The pH response of PSMA-1092 highlighted its potential in a broader field, such as for noninvasively measuring the pH value of gastric juice.<sup>51</sup> The tremendous wavelength shift, which was over a span from the NIR-II region to NIR-I, could effectively avoid the influence of the original wavelength and thus prompted the detection accuracy. Further studies of pH response applications are still underway.

To further investigate the mechanism of pH response,  $^1H$  NMR titration with deuterated trifluoroacetic acid (TFA) was performed. The protons in the aromatic ring and the *N*-alkyl donor groups displayed gradual downfield shifts (8.18 to 8.49 ppm for  $H_1$ , 6.94 to 7.82 ppm for  $H_2$ , 3.02 to 3.39 ppm for  $H_3$ , 3.05 to 3.18 ppm for  $H_4$ , and 2.40 to 2.63 ppm for  $H_5$ , Figure 3g) with an increasing amount of deuterated TFA, indicating that the electron density of the donor moiety was decreased. Based on the above data, it could be inferred that the nitrogen on the dialkylamino group tended to be protonated in an acid environment (Figure 3f), which resulted in a lower density in the electron acceptor moiety and thus inhibited the ICT effect. It should be noted that a similar phenomenon was also observed in other NIR-II fluorescent probes, in which they displayed a 150 or 120 nm hypochromic shift after exposure to an acid environment; however, such a tremendous blue shift (472 nm) and linear correlation were first reported in this study.<sup>51,52</sup>

**In Vitro Biological Properties.** To quantitatively investigate the affinity of PSMA-1092 toward PSMA, an in vitro competitive inhibition assay was performed according to reported methods.<sup>48</sup> Owing to the synergistic effect of two PSMA targeting moieties, PSMA-1092 demonstrated ultrahigh affinity to PSMA with a  $K_i$  of 80 pM, which was higher than that of other PSMA inhibitors, such as ZJ-43 (3.53 nM, under the same assay conditions) or L16 (0.65 nM).<sup>48</sup> The high affinity of the probe could effectively improve the detection sensitivity and reduce nontarget uptake, which could lead to an excellent performance in NIR-II imaging. To further evaluate the biocompatibility of PSMA-1092, an MTT assay was performed using PC3 cells. No apparent decrease in cell viability was observed with the increasing concentration (up to 50  $\mu M$ ) of PSMA-1092 (Figure S5), indicating the low toxicity of our probe. Moreover, our probe demonstrated high stability in blood; after being incubated with mice plasma for 24 h, there are no decomposed compounds detected by the HPLC method (Figure S6).

**In Vivo NIR-II Imaging of Tumor-Bearing Mice.** To further test the in vivo performance of PSMA-1092, subcutaneous LNCaP tumor-bearing mice ( $n = 3$ ) were used in NIR-II imaging. After the tail vein administration of PSMA-1092 at a dose of 2.5 mg/kg body weight, NIR-II imaging was acquired at different time points (1, 2, 4, 6, 8, 12, and 24 h, Figure 4 and Figure S7) under 792 nm laser excitation at a power density of 100 mW/cm<sup>2</sup> (1000 nm long-pass filter, 50 ms exposure time). As shown in Figure 4, PSMA-1092 accumulates

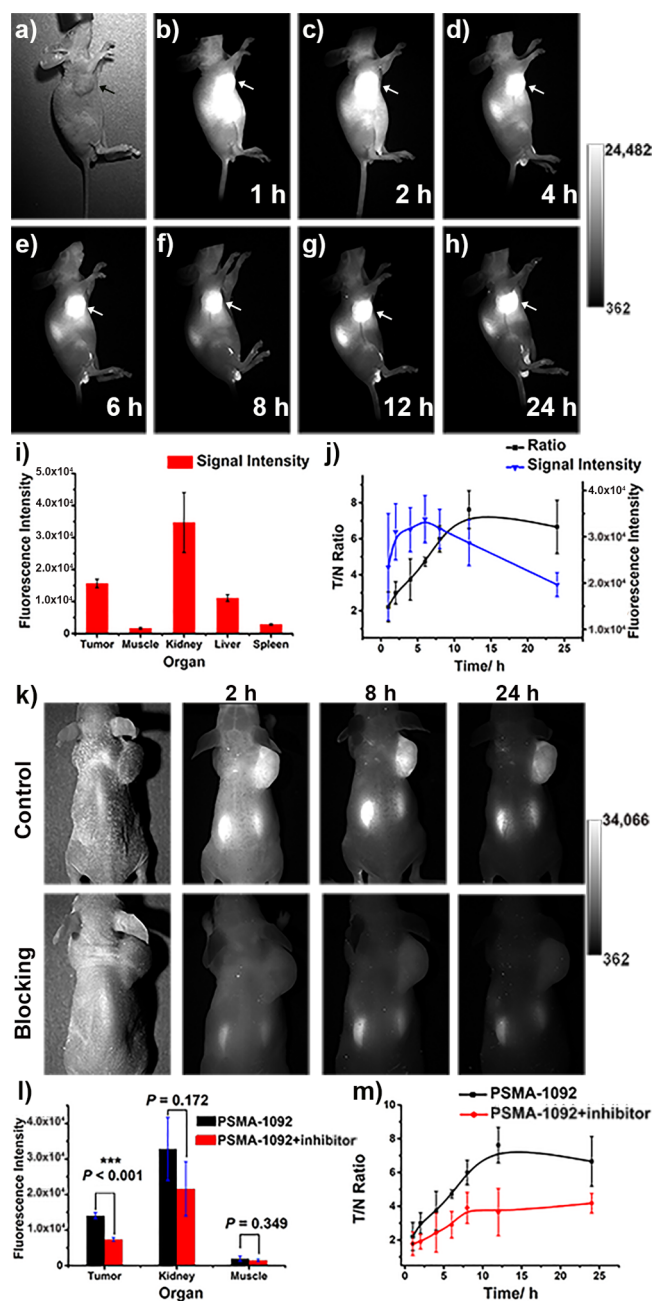


**Figure 4.** (a–h) NIR-II images of LNCaP tumor-bearing mice ( $n = 3$ ) after tail vein injection of PSMA-1092 (2.5 mg/kg) at different time points. (i) Semiquantitative analysis of PSMA-1092 biodistribution in major organs. (j) TNR (left Y axis, black line) and tumor uptake (right axis, blue line) versus time curve after intravenous injection of PSMA-1092 in tumor-bearing mice. (k) NIR-II images of LNCaP tumor-bearing mice ( $n = 3$ ) after injection of PSMA-1092 with or without 2-PMPA at different time points. (l) Quantitative analysis of PSMA-1092 biodistribution in two group mice. (m) TNR versus time curve of two group mice after tail vein injection of agents. Fluorescent intensities and T/N ratios were measured in triplicate with results given as the mean  $\pm$  standard deviation. Significance was calculated by a Student's *t* test. \*\*\* $p < 0.001$ .

in the tumor and surrounding tissue within 2 h postinjection (Figure 4c). After 4 h postinjection, the tumor was distinguished from surrounding tissue with good contrast (Figure 4d), and the high image quality was maintained at further time points (Figure 4e–h), indicating excellent imaging performance and high

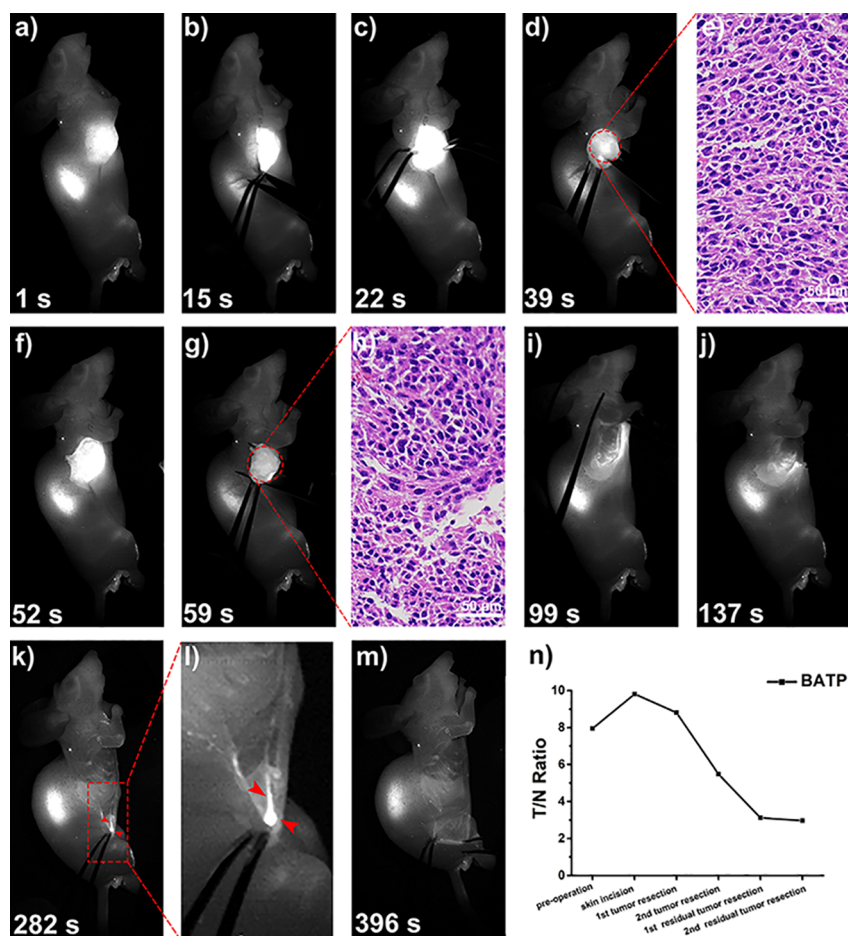


**Figure 5.** (a–d,f,g,i–m) Images of the intraoperative NIR-II imaging-guided precise tumor resection. (e,h) Histological study of two resected tumors. Scale bar: 50  $\mu\text{m}$ . (n) TNR value along the surgery ( $n = 1$ ).

stability of **PSMA-1092** in the mice model. To obtain more detailed pharmacokinetic information, a semiquantitative analysis of tumor-to-normal tissue ratio (TNR) based on the NIR-II images was performed. The maximum tumor uptake was reached at 6 h postinjection, whereas the peak value of TNR was obtained at 12 h postinjection ( $7.62 \pm 1.05$ , Figure 4j), owing to the clearance rate of **PSMA-1092** in normal tissue being faster than that in the tumor. According to the Rose criterion, an TNR of 5 is necessary to differentiate image features with 100% certainty.<sup>29,53</sup> The TNR values of **PSMA-1092** in NIR-II imaging reached  $5.99 \pm 0.72$  at 8 h postinjection and maintained a high level ( $7.62 \pm 1.05$  for 12 h and  $6.66 \pm 1.48$  for 24 h postinjection, Figure 4j) at later time points, which were both suppressing the Rose criterion and enabling excellent NIR-II image quality. Ex vivo imaging data were collected at 24 h postinjection to study the distribution of **PSMA-1092** in major organs. In addition to the tumor, a high accumulation of **PSMA-1092** in the kidney and liver (Figures S8a,c,d and S10) was observed, indicating **PSMA-1092** is mainly metabolized by the liver and excreted through the kidney system. More importantly, without the interference of skin, the fluorescence signal of muscle could rarely be detected (Figures S8b and S9), and the TNR ratio was further enhanced, achieving a value of 9.44 (Figure 4i). To study the pharmacokinetics of **PSMA-1092**, an in vivo blood clearance experiment was performed on ICR mice (8 weeks old,  $n = 3$ ). After intravenous administration of **PSMA-1092** (10 mg/kg), the fluorescence intensities of blood samples

collected from the above mice demonstrated a fast decline in the beginning (0–7 h), and the downtrend tended to be slow after 10 h postinjection (Figure S11). The ultrahigh affinity ( $K_i = 80$  pM) toward PSMA, moderate clearance rate, excellent NIR-II imaging performance, and high tumor-to-muscle ratio of **PSMA-1092** highlight its potential utilization for in vivo imaging and intraoperative fluorescence image-guided precise tumor resection in clinical practice.

To verify the specificity of **PSMA-1092** for PSMA, a blocking experiment was further performed on tumor-bearing mice ( $n = 3$  per group). NIR-II images (792 nm laser excitation, 1000 nm LP filter, and 50 ms exposure time) were obtained at selected time points after the co-injection of **2-PMPA** (a potent and selective inhibitor of glutamate carboxypeptidase II with an  $\text{IC}_{50}$  of 300 pM, 34.3 mg/kg body weight) and **PSMA-1092** (2.5 mg/kg body weight).<sup>54,55</sup> Tumor-bearing mice injected only **PSMA-1092** (2.5 mg/kg body weight) were assigned as the control group to analyze the blocking data. As shown in Figure 4k and Figure S12, in the blocking group, most of the tumor signal in living mice could be inhibited by **2-PMPA**, and semiquantitative analysis indicated that the TNR values of the control group were much higher than those of the blocking group after 6 h postinjection (Figure 4m). Further ex vivo imaging demonstrated that fluorescence signals from tumors and kidneys were successfully reduced after co-injection of **2-PMPA** and **PSMA-1092** (Figure 4l and Figure S13). These results well proved that **PSMA-1092** is a specific ligand for PSMA and has ultrahigh

affinity, which meets most of the requirements for a NIR-II imaging probe.

**Intraoperative Fluorescence Image-Guided Precise Tumor Resection.** To verify the feasibility of PSMA-1092 in intraoperative fluorescence image-guided precise tumor resection, living LNCaP tumor-bearing mice were selected to perform tumor resection study under anesthesia. According to the above imaging data, the optimal time window for surgery was selected at 24 h postinjection of PSMA-1092 (2.5 mg/kg body weight) by tail vein to obtain the lowest background signal. During the entire operation, the mouse was anesthetized by the combination gas of isoflurane and oxygen at a rate of 0.4 L/min. The tumor was resected under the NIR-II navigation, and the entire process was recorded by the imaging instrument (Figure 5 and supplementary video). First, the skin around the tumor region was dissected to expose the tumor (Figure 5b,c). Semiquantitative analysis indicated that the TNR value was increased after the incision (from 7.95 to 9.81, Figure 5n) since the removal of covering skin. Then the tumor was resected (Figure 5d,f,g) and thought to be completely removed by visible inspection. However, an intense fluorescence signal was still observed from the surrounding area (Figure 5i) with a TNR value of 5.48 (Figure 5n), indicating there was still residual tumor missed by the operation in margin. Guided by the NIR-II fluorescent imaging, the residual tumor was further resected (Figure 5j), while the healthy tissue was maintained as much as possible, with the TNR value decreased to 3.12 (Figure 5n) after resection. However, after the extended resection, a fluorescent line could still be detected from the remaining tissue (Figure 5j). More detailed inspection found a missed tiny tumor (Figure 5k,l, indicated by red arrowhead), which was further removed with no residual fluorescence signal observed by the imaging instrument (TNR = 2.97, Figure 5m,n). Histological study using hematoxylin and eosin (H&E) staining demonstrated that the resected tumor was poorly differentiated carcinoma. Overall, the outstanding tumor delineation capability highlights the promising NIR-II small-molecule probe with clinical translational potential for fluorescence image-guided precise tumor resection.

Moreover, the excellent optical properties and high affinities of PSMA-1092 make it possible to obtain a clear NIR-II image within a short exposure time (50 ms), which ensures 20 frames could be recorded in 1 s. The high frame rate of imaging could guarantee fluent signal feedback in real time, which facilitates the precise tumor resection in clinical practice.

## CONCLUSION

A novel fluorescent probe for NIR-II imaging of PCa tumors and image-guided precise tumor resection was successfully designed, synthesized, and evaluated. The probe demonstrated excellent optical properties ( $\lambda_{\max} = 1092$  nm in DMSO,  $\Phi = 6.66\%$  in PBS), ideal water solubility, prominent biocompatibility, and ultrahigh affinity ( $K_i = 80$  pM) toward PSMA, which meets most of the requirements for NIR-II imaging. Interestingly, PSMA-1092 displayed a sensitive fluorescent response to the pH value of the solution, and the fluorescence maxima shifted to 620 nm (NIR-I) from its original wavelength (NIR-II) when transferred into an acid environment. Moreover, PSMA-1092 exhibited excellent performance in the in vivo imaging of PCa mice with a good contrast and high resolution. The tumor was contoured accurately at 4 h postinjection, and the maximum of TNR reaches  $7.62 \pm 1.05$  at 12 h postinjection. More importantly, in the intraoperative NIR-II image-guided surgery using PSMA-

1092, the tumor was successfully delineated with a high spatial and temporal resolution (TNR = 9.81). After the resection of the tumor, a residual tumor in the margin missed by visible inspection was successfully detected by the NIR-II imaging, which highlighted the powerful sensitivity of our probe. In summary, as a molecular probe, PSMA-1092 meets the requirements for intraoperative NIR-II image-guided precise tumor resection, and it is a highly promising candidate for clinical practice.

## EXPERIMENTAL PROCEDURES

**General Information.** All reagents used for synthesis were purchased commercially and used without further purification unless specifically noted. Reaction processes were monitored by thin-layer chromatography (TLC) on Merck silica gel 60 F<sub>254</sub> plates (Germany). After the reactions, the coarse productions were loaded on a Bonna-Agela Technologies Co., Ltd. flash column silica-CS (20–80 g, 12.6 bar, China) and purified by Bonna-Agela Technologies Co., Ltd. FLEXA modular preparative chromatography system (China). <sup>1</sup>H and <sup>13</sup>C NMR spectra were performed on a Bruker Avance III (400 or 100 MHz, German), JEOL JNM-ECZ400R/S1 (400 or 100 MHz, Japan), or JNM-ECZ600R/S3 (600 or 150 MHz, Japan) NMR spectrometer in CDCl<sub>3</sub>, DMSO-*d*<sub>6</sub>, or trifluoroacetic acid-*d* solution at room temperature unless further noted. Chemical shifts were reported in parts per million (ppm) compared with tetramethylsilane ( $\delta$  0.00, s). Coupling constants were reported in hertz (Hz). Multiplicities were reported as s (singlet), d (doublet), t (triplet), and m (multiplet). MS spectra were collected on Thermo Scientific LCQ FLEET (ESI) mass spectrometer (USA). High-resolution mass spectra were recorded on Thermo scientific Q-Eactive (ESI) mass spectrometer (USA). The purity of PSMA-1092 was determined by HPLC method, and the purity was greater than 95%. UV–vis–NIR spectra were performed on a Shimadzu UV-3600 UV–vis–NIR spectrophotometer (Japan). Fluorescence spectra and fluorescence quantum yields were recorded on an Edinburgh Instruments FLS980 fluorescence spectrometer (UK). LNCaP and PC3 cell lines were obtained from the Chinese Academy of Sciences Typical Culture Collection (Shanghai, China). The quantitative binding affinities were determined by an in vitro inhibition assay using the lysate of LNCaP cells according to previously reported works.<sup>48</sup> In vivo NIR-II imaging was performed on a Princeton Instruments NIRvana 640 InGaAs charge-coupled device camera (USA) coupled to a lens of a Schneider Kreuznach SWIRON 2.8/50 high transparency instrument in the NIR-II spectrum (Germany). A Thorlabs FEL1000 LP 1000 nm long-pass filter (USA) was fixed on the end of the lens to filter the excitation light. LNCaP tumor-bearing mice were purchased from the Institute of Laboratory Animals Science, CAMS & PUMC (China). The tissue embedding, sectioning, H&E staining, and microscope photography were entrusted to Wuhan Servicebio Technology Co., Ltd. (China).

**Chemistry.** 3-((4-Bromophenyl)(methyl)amino)propanoic Acid (**2**). To a mixture of **1** (7.80 g, 40.00 mmol, 1 equiv) in acetic acid (20% in H<sub>2</sub>O, 50 mL) was added acrylic acid (3.75 g, 52.00 mmol, 1.3 equiv). The reaction was refluxed overnight and monitored by TLC. The mixture was cooled to room temperature and extracted by CH<sub>2</sub>Cl<sub>2</sub> (15 mL  $\times$  3). The combined organic layer was dried over MgSO<sub>4</sub> and concentrated in vacuum. The crude product was purified by silica gel column chromatography (petroleum/ethyl acetate = 2/1, v/v) to give **2** as a yellow solid (9.70 g, 94.5%). <sup>1</sup>H NMR (600 MHz, CDCl<sub>3</sub>):  $\delta$  7.32 (d, *J* = 9.0 Hz, 2H), 6.64 (d, *J* = 9.0 Hz, 2H), 3.65 (t, *J* = 7.1 Hz, 2H), 2.92 (s, 3H), 2.61 (t, *J* = 7.1 Hz, 2H). MS: *m/z* calcd for [M + H]<sup>+</sup> 258.0, found 258.0.

*tert*-Butyl 3-((4-Bromophenyl)(methyl)amino)propanoate (**3**). To a suspension of **2** (7.96 g, 31.00 mmol, 1 equiv) in CH<sub>2</sub>Cl<sub>2</sub> (50 mL) were added in succession *tert*-butanol (3.45 g, 46.52 mmol, 1.5 equiv), dicyclohexylcarbodiimide (9.59 g, 46.50 mmol, 1.5 equiv) and 4-dimethylaminopyridine (0.19 g, 1.60 mmol, 0.05 equiv). The mixture was maintained at room temperature overnight and monitored by TLC. The reaction mixture was filtrated, and the solution was concentrated in vacuum. The crude product was purified by silica gel column

chromatography (petroleum ether/ethyl acetate = 6/1, v/v) to give **3** as a yellow oil (4.20 g, 43.2%).  $^1\text{H NMR}$  (400 MHz,  $\text{CDCl}_3$ ):  $\delta$  7.30 (d,  $J$  = 9.0 Hz, 2H), 6.62 (s, 2H), 3.60 (t,  $J$  = 7.2 Hz, 2H), 2.91 (s, 3H), 2.46 (t,  $J$  = 7.2 Hz, 2H), 1.43 (s, 9H).  $^{13}\text{C NMR}$  (151 MHz,  $\text{CDCl}_3$ ):  $\delta$  171.49, 139.88, 131.93, 114.16, 108.61, 80.85, 55.82, 38.34, 35.00, 28.14. HRMS:  $m/z$  calcd for  $[\text{M} + \text{H}]^+$  314.0677, found 314.0750.

**tert-Butyl 3-(Methyl(4-(tributylstannyl)phenyl)amino)propanoate (4).** To the solution of **3** (4.00 g, 12.70 mmol, 1 equiv) in toluene (50 mL) was added  $\text{Pd}(\text{PPh}_3)_4$  (1.47 g, 1.27 mmol, 0.1 equiv). Hexabutylstannane (7.43 g, 12.74 mmol, 1 equiv) was then added under  $\text{N}_2$ . The reaction was stirred at 120 °C for 2 h and monitored by TLC. After being cooled to room temperature, to the mixture was added  $\text{H}_2\text{O}$  and extracted by diethyl ether (15 mL  $\times$  3). The combined organic layers were dried over  $\text{MgSO}_4$  and concentrated under vacuum to give **4** as a brown oil, which was used for the next step without further purification.

**Di-tert-butyl 3,3'-((5,6-Dinitrobenzo[*c*][1,2,5]thiadiazole-4,7-diy)bis(4,1-phenylene)bis(methylazanediy))dipropionate (5).** To the mixture of 4,7-dibromo-5,6-dinitrobenzo[*c*][1,2,5]thiadiazole (1.23 g, 3.21 mmol, 1 equiv) and  $\text{PdCl}_2(\text{PPh}_3)_2$  (0.45 g, 0.64 mmol, 0.2 equiv) in toluene (50 mL) was added **4** under  $\text{N}_2$ . The reaction was stirred at 120 °C for 2 h and monitored by TLC. The solvent was removed by evaporation in vacuum, and the residue was purified by silica gel column chromatography (petroleum ether/ethyl acetate = 5/1, v/v) to give **5** as a purplish red solid (171.0 mg, 7.7%).  $^1\text{H NMR}$  (600 MHz,  $\text{CDCl}_3$ ):  $\delta$  7.51 (d,  $J$  = 8.7 Hz, 2H), 6.93 (s, 2H), 3.72 (t,  $J$  = 7.2 Hz, 2H), 3.07 (s, 3H), 2.59 (t,  $J$  = 6.9 Hz, 2H), 1.45 (s, 9H).  $^{13}\text{C NMR}$  (101 MHz,  $\text{CDCl}_3$ ):  $\delta$  171.36, 153.58, 149.95, 142.10, 130.71, 127.71, 117.77, 112.01, 81.04, 48.27, 38.36, 33.41, 28.17. HRMS:  $m/z$  calcd for  $[\text{M} + \text{H}]^+$  693.2628, found 693.2703.

**Di-tert-butyl 3,3'-((5,6-Diaminobenzo[*c*][1,2,5]thiadiazole-4,7-diy)bis(4,1-phenylene)bis(methylazanediy))dipropionate (6).** To the solution of **5** (327.2 mg, 0.47 mmol, 1 equiv) in acetic acid (40 mL) was added iron powder (1.32 g, 23.50 mmol, 50 equiv). The mixture was stirred at 100 °C and monitored by TLC. After being cooled to room temperature, the reaction was filtered and the filtrate was added to ice water and neutralized by  $\text{NaHCO}_3$ . The mixture was then extracted by  $\text{CH}_2\text{Cl}_2$  (15 mL  $\times$  3). The combined organic layers were dried over  $\text{Na}_2\text{SO}_4$  and concentrated under vacuum. The crude product was purified by silica gel column chromatography (petroleum ether/ethyl acetate = 3/1, v/v) to give **6** as a brown solid (106.8 mg, 36.2%).  $^1\text{H NMR}$  (400 MHz,  $\text{CDCl}_3$ ):  $\delta$  7.47 (d,  $J$  = 7.9 Hz, 2H), 6.93 (s, 2H), 4.10 (s, 1H), 3.72 (t,  $J$  = 7.0 Hz, 2H), 3.04 (s, 3H), 2.57 (s, 2H), 1.47 (s, 9H).  $^{13}\text{C NMR}$  (151 MHz,  $\text{CDCl}_3$ ):  $\delta$  171.68, 151.75, 148.33, 138.18, 131.26, 122.64, 113.75, 112.88, 80.82, 48.66, 38.46, 33.31, 28.20. HRMS:  $m/z$  calcd for  $[\text{M} + \text{H}]^+$  633.3145, found 633.3221.

**Compound 7.** To the solution of **6** (106.5 mg, 0.17 mmol, 1 equiv) in dry pyridine (20 mL) were added in succession  $\text{PhNSO}$  (165.6 mg, 1.19 mmol, 7 equiv) and  $\text{TMSCl}$  (2.40 g, 22.07 mmol, 130 equiv). The reaction was stirred at 80 °C overnight and monitored by TLC. After being cooled to room temperature, the above mixture was poured into ice water and extracted by  $\text{CH}_2\text{Cl}_2$  (15 mL  $\times$  3). The combined organic layers were dried over  $\text{Na}_2\text{SO}_4$  and concentrated under vacuum. The residue was purified by silica gel column chromatography (petroleum ether/ethyl acetate = 6/1, v/v) to give **7** as a green solid (30.5 mg, 27.2%).  $^1\text{H NMR}$  (400 MHz,  $\text{CDCl}_3$ ):  $\delta$  8.31 (d,  $J$  = 8.4 Hz, 2H), 7.14 (s, 2H), 3.78 (t,  $J$  = 7.3 Hz, 2H), 3.15 (s, 3H), 2.69 (s, 2H), 1.46 (s, 9H).  $^{13}\text{C NMR}$  (101 MHz,  $\text{CDCl}_3$ ):  $\delta$  171.55, 152.85, 148.84, 133.10, 123.81, 119.99, 112.01, 80.89, 48.53, 38.60, 33.35, 28.21. HRMS:  $m/z$  calcd for  $[\text{M} + \text{H}]^+$  661.2552, found 661.2625.

**Compound 8.** To the solution of **7** (30.5 mg, 0.046 mmol, 1 equiv) in 5 mL of  $\text{CH}_2\text{Cl}_2$  was added 5 mL of TFA. The reaction mixture was stirred at room temperature for 4 h and monitored by TLC. The solution was removed by evaporation in vacuum. The residue was added to 15 mL of  $\text{CH}_2\text{Cl}_2$  and ultrasonically vibrated for 5 min. The solid was collected by filtration and washed with 5 mL of  $\text{CH}_2\text{Cl}_2$  and 5 mL of petroleum ether. Compound **8** was obtained as a dark green solid (25.1 mg, 100%).  $^1\text{H NMR}$  (400 MHz,  $\text{DMSO}-d_6$ ):  $\delta$  8.18 (d,  $J$  = 8.4 Hz, 2H), 6.96 (d,  $J$  = 8.4 Hz, 2H), 3.74 (t,  $J$  = 7.0 Hz, 2H), 3.04 (s, 3H), 2.56 (t,  $J$  = 7.0 Hz, 2H).  $^{13}\text{C NMR}$  (101 MHz,  $\text{DMSO}-d_6$ ):  $\delta$  173.60,

152.54, 149.00, 133.55, 123.92, 119.36, 112.22, 48.43, 38.53, 32.10. HRMS:  $m/z$  calcd for  $[\text{M} + \text{H}]^+$  549.1300, found 549.1161.

**Compound 9.** To the suspension of **8** (25.1 mg, 0.046 mmol, 1 equiv) in  $\text{CH}_2\text{Cl}_2$  (50 mL) were added 2,3,5,6-tetrafluorophenol (18.3 mg, 0.11 mmol, 2.4 equiv) and  $N,N'$ -dicyclohexylcarbodiimide (22.7 mg, 0.11 mmol, 2.4 equiv). The reaction mixture was stirred at room temperature for 5 h and monitored by TLC. The solvent was removed by evaporation in vacuum, and the residue was purified by silica gel column chromatography (petroleum ether/ $\text{CH}_2\text{Cl}_2$  = 1/5, v/v) to give **9** as a blue solid (25.9 mg, 67.4%).  $^1\text{H NMR}$  (400 MHz,  $\text{CDCl}_3$ ):  $\delta$  8.47 (d,  $J$  = 8.8 Hz, 2H), 7.87 (d,  $J$  = 8.5 Hz, 2H), 7.07–6.96 (m, 1H), 3.96 (t,  $J$  = 7.4 Hz, 2H), 3.41 (t,  $J$  = 7.3 Hz, 2H), 3.32 (s, 3H).  $^{13}\text{C NMR}$  (101 MHz,  $\text{CDCl}_3$ ):  $\delta$  168.19, 152.85, 148.44, 139.89, 133.23, 124.34, 120.03, 112.13, 103.68, 103.45, 102.98, 55.83, 38.83, 35.00. HRMS:  $m/z$  calcd for  $[\text{M} + \text{H}]^+$  845.1173, found 845.1249.

**Compound 10.** To the solution of **9** (25.9 mg, 0.031 mmol, 1 equiv) in  $\text{CH}_2\text{Cl}_2$  (50 mL) were added in succession *tert*-butyl Glu-urea-Lys (35.9 mg, 0.074 mmol, 2.4 equiv) and  $\text{Et}_3\text{N}$  (12.5 mg, 0.074 mmol, 2.4 equiv). The reaction mixture was stirred at room temperature for 6 h and monitored by TLC. The solvent was removed by evaporation in vacuum, and the residue was purified by silica gel column chromatography (petroleum ether/ethyl acetate = 1/5, v/v) to give **10** as a green solid (28.5 mg, 61.3%).  $^1\text{H NMR}$  (400 MHz,  $\text{CDCl}_3$ ):  $\delta$  8.42 (d,  $J$  = 8.6 Hz, 2H), 8.05 (d,  $J$  = 8.4 Hz, 2H), 6.95 (s, 1H), 4.36–4.28 (m, 2H), 3.98 (ddt,  $J$  = 34.8, 13.0, 6.9 Hz, 2H), 3.31 (s, 3H), 3.06 (s, 1H), 2.85 (s, 1H), 2.40 (t,  $J$  = 7.8 Hz, 2H), 2.17–2.02 (m, 2H), 1.97–1.54 (m, 6H), 1.49 (s, 2H), 1.43 (s, 9H), 1.41 (s, 9H), 1.41 (s, 9H).  $^{13}\text{C NMR}$  (101 MHz,  $\text{CDCl}_3$ ):  $\delta$  172.83, 172.49, 172.20, 171.58, 157.28, 82.09, 81.62, 80.50, 77.30, 67.98, 60.38, 53.39, 53.24, 39.19, 32.51, 31.69, 30.44, 28.81, 28.18, 28.09, 25.65, 22.62, 21.01, 14.22. HRMS:  $m/z$  calcd for  $[\text{M}]^+$  1531.8308, found 1531.7543.

**Compound PSMA-1092.** To the solution of **10** (28.5 mg, 0.019 mmol, 1 equiv) in 5 mL of  $\text{CH}_2\text{Cl}_2$  was added 5 mL of TFA. The reaction mixture was stirred at room temperature for 4 h. The solvent was removed by evaporation in vacuum, and the residue was added to 10 mL of diethyl ether and a dark green precipitate was formed. Diethyl ether was removed carefully, and 10 mL of petroleum ether was added to wash the precipitate. After petroleum ether was removed, the precipitate was allowed to be dried off to give **PSMA-1092** as a green solid (21.5 mg, 98.4%).  $^1\text{H NMR}$  (600 MHz,  $\text{DMSO}-d_6$ ):  $\delta$  8.18 (d,  $J$  = 8.5 Hz, 2H), 7.98 (t,  $J$  = 5.5 Hz, 1H), 6.95 (d,  $J$  = 8.6 Hz, 2H), 6.31 (m, 2H), 4.10 (td,  $J$  = 8.1, 5.2 Hz, 1H), 4.03 (q,  $J$  = 7.1 Hz, 3H), 3.72 (d,  $J$  = 7.2 Hz, 2H), 3.03 (d,  $J$  = 16.1 Hz, 5H), 2.40 (t,  $J$  = 7.0 Hz, 2H), 2.24 (qdd,  $J$  = 16.4, 9.1, 6.2 Hz, 2H), 1.91 (s, 2H), 1.75–1.61 (m, 2H), 1.40 (tt,  $J$  = 7.9, 4.5 Hz, 2H), 1.30 (q,  $J$  = 7.7, 5.6 Hz, 2H).  $^{13}\text{C NMR}$  (151 MHz,  $\text{DMSO}-d_6$ ):  $\delta$  174.43, 174.06, 173.61, 170.30, 170.24, 157.20, 151.91, 148.38, 132.93, 118.73, 111.48, 59.65, 52.18, 51.57, 48.46, 38.35, 37.94, 32.86, 31.72, 29.81, 28.67, 27.45, 22.57, 20.66, 13.99. HRMS:  $m/z$  calcd for  $[\text{M} - \text{H}]^-$  1149.3848, found 1149.3775.

**Method. Purity Determination.** The purity of **PSMA-1092** was determined by HPLC. **PSMA-1092** aqueous solution (500  $\mu\text{L}$ , containing 5% DMSO) was analyzed by a Bonna-Agela Technologies Venusil MP C18 reverse-phase column (5  $\mu\text{m}$ , 4.6 mm  $\times$  250 mm) and eluted at a flow rate of 1.0 mL/min. Mobile phase A was water (with 0.1% TFA), and mobile phase B was acetonitrile (A/B = 73/27, v/v). HPLC was performed on a Hitachi Primaide system (Japan) equipped with an SPD-20A UV detector ( $\lambda$  = 600 nm).

Fluorescence penetration: **PSMA-1092** aqueous solution (0.5 mg/mL, containing 5% DMSO) was filled into a capillary glass tube (1.5 mm  $\times$  100 mm) and fixed on the imaging platform. Different chicken breast tissue with known thickness was covered upon the fixed capillary glass tube, and the NIR-II images were acquired subsequently.

**NMR Titration.** **PSMA-1092** (8.33 mg) was dissolved in 1.5 mL of  $\text{DMSO}-d_6$ , and its  $^1\text{H NMR}$  spectrum was recorded on a JNMECZ600R/S3 NMR spectrometer (600 MHz, Japan) at 30 °C. Then various amounts of TFA-*d* were added successively with the final volumes of 20, 45, 80, 140, 210, 310, and 360  $\mu\text{L}$  for each time. After each addition of TFA-*d*, the  $^1\text{H NMR}$  spectrum of the sample was recorded.

**Cell Culture.** LNCaP and PC3 cells were cultured in Sigma RPMI-1640 media (USA) supplemented with 10% fetal bovine serum and 1% penicillin–streptomycin solution. All the cells were maintained in a humidified environment with 5% CO<sub>2</sub> at 37 °C in an incubator.

**In Vitro Inhibition Assay.** To quantitatively analyze the binding affinity of PSMA-1092 to PSMA, an in vitro inhibition assay was performed according to a previous study with slight modification.<sup>1</sup> First, 12.5 μL of *N*-acetylaspartylglutamate (8 μM) and 12.5 μL of PSMA-1092 solution (variable concentration covering 0.01 nM to 1 μM) were added into the lysates of LNCaP cell extracts (25 μL), and the above mixture was incubated for 120 min. The glutamate concentration was measured by incubation with a working solution (50 μL) of the Amplex Red glutamic acid kit for 30 min, and the fluorescence intensities were recorded by a plate reader (excitation = 530 nm and emission = 590 nm). IC<sub>50</sub> values were determined from the inhibition curve at the concentration at which enzyme activity was inhibited by 50%, and enzyme inhibitory constants (*K<sub>i</sub>* values) were calculated using the Cheng–Prusoff conversion. Assays were performed in triplicate.

**MTT Assay.** PC-3 cells were seeded into a 96-well plate and incubated at 37 °C with 5% CO<sub>2</sub> for 24 h. Then the cells were treated with different concentration of PSMA-1092 (10.0, 20.0, 25.3, 40.0, and 50.0 μM) and PBS as the control for 24 incubation. After incubation, MTT solution (5 mg/mL) was added, and the cells were kept incubating for another 4 h. After the culture media were removed by centrifugation, 300 μL of DMSO was added. The absorbance of each well was measured at 570 nm using a 1420 Multiabel counter for assessing the viability of living cells.

**In Vitro Stability in Plasma.** One hundred microliters of PSMA-1092 aqueous solution was added into 1 mL of mice plasma (100 μM), and the above mixture was incubated at 37 °C. A 100 μL sample was collected at selected time points (1, 2, 3, 12, 24 h) and treated with 300 μL of acetonitrile. After centrifugation and filtration, 90 μL of supernatant was collected and added 160 μL of H<sub>2</sub>O. The above mixture was subjected to HPLC analysis, and the purities of PSMA-1092 were determined using acetonitrile/H<sub>2</sub>O = 27/73 with a flow rate of 1 mL/min.

**In Vivo Blood Clearance.** After intravenous administration of PSMA-1092 (10 mg/kg, ICR, 8 weeks old), the blood sample was collected at selected time points and stored in a centrifuge tube (2.5 mL) with heparin sodium. After centrifugation, the NIR-II images of 50 μL blood sample supernatants were acquired under the same condition (100 mW/cm<sup>2</sup> power density, 1000 nm long-pass filter, 500 ms exposure time), and the fluorescence intensities were analyzed by ImageJ.

**In Vivo NIR-II Imaging.** To perform in vivo NIR-II fluorescence imaging, LNCaP tumor-bearing mice were administered PSMA-1092 (2.5 mg/kg) intravenously, and the NIR-II imaging was performed at 1, 2, 4, 6, 8, 12, and 24 h postinjection under 792 nm laser excitation at a power density of 100 mW/cm<sup>2</sup> (1000 nm long-pass filter, 50 ms exposure time). Mice were anesthetized by the combination gas of isoflurane and oxygen at a rate of 0.4 L/min and remained under anesthesia for the whole process. The NIR-II images were analyzed with the open-source software ImageJ.

**Intraoperative Image-Guided Tumor Resection.** LNCaP tumor-bearing mice were intravenously injected with PSMA-1092 (2.5 mg/kg) and received surgery at 24 h postinjection. Mice were anesthetized by the combination gas of isoflurane and oxygen at a rate of 0.4 L/min before the operation and remained under anesthesia for the surgery. The tumor was removed under the guidance of NIR-II images, and the whole process was recorded by the imaging instrument. The NIR-II images were analyzed on the open-source software ImageJ.

**Data Availability.** The data supporting the results of this study are available in this article and its Supporting Information. The raw data are available in at [10.6084/m9.figshare.13520072.v1](https://doi.org/10.6084/m9.figshare.13520072.v1).

**Laboratory Animals.** All protocols requiring the use of animals conformed to the China Animal Management Regulations (2017 edition) and were approved by the animal care committee of Beijing Normal University.

## ■ ASSOCIATED CONTENT

### Supporting Information

The Supporting Information is available free of charge at <https://pubs.acs.org/doi/10.1021/acs.jmedchem.1c00444>.

Additional figures, <sup>1</sup>H NMR, <sup>13</sup>C NMR, and HRMS spectra (PDF)

Tumor resection under NIR-II navigation video of PSMA-1092 (AVI, AVI)

Molecular formula strings (CSV)

## ■ AUTHOR INFORMATION

### Corresponding Authors

**Mengchao Cui** – Key Laboratory of Radiopharmaceuticals, Ministry of Education, College of Chemistry, Beijing Normal University, Beijing 100875, China; Center for Advanced Materials Research, Advanced Institute of Natural Sciences, Beijing Normal University at Zhuhai, Zhuhai 519087, China; [orcid.org/0000-0002-3488-7864](https://orcid.org/0000-0002-3488-7864); Phone: +86-13811995064; Email: [cmc@bnu.edu.cn](mailto:cmc@bnu.edu.cn)

**Zhenhua Hu** – CAS Key Laboratory of Molecular Imaging, Beijing Key Laboratory of Molecular Imaging, The State Key Laboratory of Management and Control for Complex Systems, Institute of Automation, Chinese Academy of Sciences, Beijing 100190, China; Phone: +86-10-82544536; Email: [zhenhua.hu@ia.ac.cn](mailto:zhenhua.hu@ia.ac.cn)

### Authors

**Longfei Zhang** – Key Laboratory of Radiopharmaceuticals, Ministry of Education, College of Chemistry, Beijing Normal University, Beijing 100875, China

**Xiaojing Shi** – CAS Key Laboratory of Molecular Imaging, Beijing Key Laboratory of Molecular Imaging, The State Key Laboratory of Management and Control for Complex Systems, Institute of Automation, Chinese Academy of Sciences, Beijing 100190, China

**Yuying Li** – Key Laboratory of Radiopharmaceuticals, Ministry of Education, College of Chemistry, Beijing Normal University, Beijing 100875, China

**Xiaojiang Duan** – Department of Nuclear Medicine, Peking University First Hospital, Beijing 100034, China

**Zeyu Zhang** – School of Medical Science and Engineering, Beihang University, Beijing 100191, China

**Hualong Fu** – Key Laboratory of Radiopharmaceuticals, Ministry of Education, College of Chemistry, Beijing Normal University, Beijing 100875, China

**Xing Yang** – Department of Nuclear Medicine, Peking University First Hospital, Beijing 100034, China; [orcid.org/0000-0001-5186-4990](https://orcid.org/0000-0001-5186-4990)

**Jie Tian** – CAS Key Laboratory of Molecular Imaging, Beijing Key Laboratory of Molecular Imaging, The State Key Laboratory of Management and Control for Complex Systems, Institute of Automation, Chinese Academy of Sciences, Beijing 100190, China

Complete contact information is available at:

<https://pubs.acs.org/doi/10.1021/acs.jmedchem.1c00444>

### Author Contributions

M.C. and L.Z. conceived and designed the experiment. L.Z. synthesized and characterized PSMA-1092. Optical properties were determined by L.Z. MTT assay was performed by Y.L. In vitro competitive inhibition assay was performed by X.D. Animal studies were performed by L.Z., X.S., M.C., H.F., and Z.Z. M.C.,

Z.H., L.Z., and X.S. analyzed the data. M.C., Z.H., X.Y., and J.T. provided reagents, materials, and experiment instruments. M.C., Z.H., L.Z., X.S., and H.F. wrote the paper. L.Z. and X.S. contributed equally to this work.

## Notes

The authors declare no competing financial interest.

## ACKNOWLEDGMENTS

This work was supported by the National Natural Science Foundation of China (NSFC) (Nos. U1967221, 22022601, and 81671759), Beijing Natural Science Foundation (7182089 and JQ19027), Beijing Nova Program (Z181100006218046), and the innovative research team of high-level local universities in Shanghai.

## ABBREVIATIONS

D–A–D, donor–acceptor–donor; DCC, *N,N'*-dicyclohexylcarbodiimide; DCM, dichloromethane; DMAP, 4-dimethylaminopyridine; DMSO, dimethyl sulfoxide; FDA, food and drug administrator; Glu-urea-Lys, (*S*)-3-(carboxyformamido)-2-(3-(carboxymethyl) ureido) propanoic acid; Hz, hertz; HRMS, high-resolution mass spectrometry; ICG, indocyanine green; ICT, intramolecular charge transfer; LP, long-pass; MS, mass spectrometry; NIR-I, near-infrared window I; NIR-II, near-infrared window II; PCA, prostate cancer; ppm, parts per million; PhNSO, *N*-sulfynylaniline; PSMA, prostate-specific membrane antigen; TLC, thin-layer chromatography; TMSCl, trimethyl chlorosilane; TFA, trifluoroacetic acid; TNR, tumor-to-normal tissue ratio

## REFERENCES

- (1) Bray, F.; Ferlay, J.; Soerjomataram, I.; Siegel, R. L.; Torre, L. A.; Jemal, A. Global cancer statistics 2018: GLOBOCAN estimates of incidence and mortality worldwide for 36 cancers in 185 countries. *Ca-Cancer J. Clin.* **2018**, *68* (6), 394–424.
- (2) Skolarus, T. A.; Wolf, A. M.; Erb, N. L.; Brooks, D. D.; Rivers, B. M.; Underwood, W., 3rd; Salner, A. L.; Zelefsky, M. J.; Aragon-Ching, J. B.; Slovin, S. F.; Wittmann, D. A.; Hoyt, M. A.; Sinibaldi, V. J.; Chodak, G.; Pratt-Chapman, M. L.; Cowens-Alvarado, R. L. American Cancer Society prostate cancer survivorship care guidelines. *Ca-Cancer J. Clin.* **2014**, *64* (4), 225–249.
- (3) Fizazi, K.; Scher, H. I.; Molina, A.; Logothetis, C. J.; Chi, K. N.; Jones, R. J.; Staffurth, J. N.; North, S.; Vogelzang, N. J.; Saad, F.; Mainwaring, P.; Harland, S.; Goodman, O. B.; Sternberg, C. N.; Li, J. H.; Kheoh, T.; Haqq, C. M.; de Bono, J. S. Abiraterone acetate for treatment of metastatic castration-resistant prostate cancer: final overall survival analysis of the COU-AA-301 randomised, double-blind, placebo-controlled phase 3 study. *Lancet Oncol.* **2012**, *13* (10), 983–992.
- (4) Olson, W. C.; Heston, W. D.; Rajasekaran, A. K. Clinical trials of cancer therapies targeting prostate-specific membrane antigen. *Rev. Recent Clin. Trials* **2007**, *2* (3), 182–190.
- (5) Fizazi, K.; Tran, N.; Fein, L.; Matsubara, N.; Rodriguez-Antolin, A.; Alekseev, B. Y.; Ozguroglu, M.; Ye, D.; Feyereabend, S.; Protheroe, A.; Sultur, G.; Luna, Y.; Li, S.; Mundle, S.; Chi, K. N. Abiraterone acetate plus prednisone in patients with newly diagnosed high-risk metastatic castration-sensitive prostate cancer (LATITUDE): final overall survival analysis of a randomised, double-blind, phase 3 trial. *Lancet Oncol.* **2019**, *20* (5), 686–700.
- (6) Lu-Yao, G. L.; Albertsen, P. C.; Moore, D. F.; Shih, W.; Lin, Y.; DiPaola, R. S.; Yao, S. L. Fifteen-year survival outcomes following primary androgen-deprivation therapy for localized prostate cancer. *JAMA Int. Med.* **2014**, *174* (9), 1460–1467.
- (7) Fowler, J. E.; Terrell, F. L.; Renfro, L. D. Co-Morbidities and Survival of Men with Localized Prostate Cancer Treated with Surgery or Radiation Therapy. *J. Urol.* **1996**, *156*, 1714–1718.
- (8) Preston, M. A.; Breau, R. H.; Lantz, A. G.; Morash, C.; Gerridzen, R. G.; Doucette, S.; Mallick, R.; Eastham, J. A.; Cagiannos, I. The association between nerve sparing and a positive surgical margin during radical prostatectomy. *Urol. Oncol.* **2015**, *33* (1), 18.e1.
- (9) Nakajima, T.; Mitsunaga, M.; Bander, N. H.; Heston, W. D.; Choyke, P. L.; Kobayashi, H. Targeted, activatable, in vivo fluorescence imaging of prostate-specific membrane antigen (PSMA) positive tumors using the quenched humanized J591 antibody-indocyanine green (ICG) conjugate. *Bioconjugate Chem.* **2011**, *22* (8), 1700–1705.
- (10) Stephenson, A. J.; Eggener, S. E.; Hernandez, A. V.; Klein, E. A.; Kattan, M. W.; Wood, D. P., Jr.; Rabah, D. M.; Eastham, J. A.; Scardino, P. T. Do margins matter? The influence of positive surgical margins on prostate cancer-specific mortality. *Eur. Urol.* **2014**, *65* (4), 675–680.
- (11) Eastham, J. A.; Kuroiwa, K.; Otori, M.; Serio, A. M.; Gorbonos, A.; Maru, N.; Vickers, A. J.; Slawin, K. M.; Wheeler, T. M.; Reuter, V. E.; Scardino, P. T. Prognostic significance of location of positive margins in radical prostatectomy specimens. *Urology* **2007**, *70* (5), 965–969.
- (12) Hensbergen, A. W.; van Willigen, D. M.; van Beurden, F.; van Leeuwen, P. J.; Buckle, T.; Schottelius, M.; Maurer, T.; Wester, H.-J.; van Leeuwen, F. W. B. Image-Guided Surgery: Are We Getting the Most Out of Small-Molecule Prostate-Specific-Membrane-Antigen-Targeted Tracers? *Bioconjugate Chem.* **2020**, *31* (2), 375–395.
- (13) Andriole, G. L. Do Margins Matter? The Prognostic Significance of Positive Surgical Margins in Radical Prostatectomy Specimens. *Yearb. Urol.* **2008**, *2008*, 157–158.
- (14) Costello, A. J. Considering the role of radical prostatectomy in 21st century prostate cancer care. *Nat. Rev. Urol.* **2020**, *17* (3), 177–188.
- (15) Smith, J. A. Quality of life and satisfaction with outcome among prostate-cancer survivors. *Urol. Oncol.-semin. Ori.* **2008**, *26*, 685.
- (16) Cui, M. Past and recent progress of molecular imaging probes for beta-amyloid plaques in the brain. *Curr. Med. Chem.* **2013**, *21* (1), 82–112.
- (17) James, M. L.; Gambhir, S. S. A molecular imaging primer: modalities, imaging agents, and applications. *Physiol. Rev.* **2012**, *92* (2), 897–965.
- (18) Hu, Z.; Zhao, M.; Qu, Y.; Zhang, X.; Zhang, M.; Liu, M.; Guo, H.; Zhang, Z.; Wang, J.; Yang, W.; Tian, J. In Vivo 3-Dimensional Radiopharmaceutical-Excited Fluorescence Tomography. *J. Nucl. Med.* **2017**, *58* (1), 169–174.
- (19) Liu, M.; Zheng, S.; Zhang, X.; Guo, H.; Shi, X.; Kang, X.; Qu, Y.; Hu, Z.; Tian, J. Cerenkov luminescence imaging on evaluation of early response to chemotherapy of drug-resistant gastric cancer. *Nano-medicine* **2018**, *14* (1), 205–213.
- (20) Sun, Y.; Qu, C.; Chen, H.; He, M.; Tang, C.; Shou, K.; Hong, S.; Yang, M.; Jiang, Y.; Ding, B.; Xiao, Y.; Xing, L.; Hong, X.; Cheng, Z. Novel benzo-bis(1,2,5-thiadiazole) fluorophores for in vivo NIR-II imaging of cancer. *Chem. Sci.* **2016**, *7* (9), 6203–6207.
- (21) Zhu, S.; Yang, Q.; Antaris, A. L.; Yue, J.; Ma, Z.; Wang, H.; Huang, W.; Wan, H.; Wang, J.; Diao, S.; Zhang, B.; Li, X.; Zhong, Y.; Yu, K.; Hong, G.; Luo, J.; Liang, Y.; Dai, H. Molecular imaging of biological systems with a clickable dye in the broad 800- to 1,700-nm near-infrared window. *Proc. Natl. Acad. Sci. U. S. A.* **2017**, *114* (5), 962–967.
- (22) Wan, H.; Yue, J.; Zhu, S.; Uno, T.; Zhang, X.; Yang, Q.; Yu, K.; Hong, G.; Wang, J.; Li, L.; Ma, Z.; Gao, H.; Zhong, Y.; Su, J.; Antaris, A. L.; Xia, Y.; Luo, J.; Liang, Y.; Dai, H. A bright organic NIR-II nanofluorophore for three-dimensional imaging into biological tissues. *Nat. Commun.* **2018**, *9* (1), 1171.
- (23) Ding, B.; Xiao, Y.; Zhou, H.; Zhang, X.; Qu, C.; Xu, F.; Deng, Z.; Cheng, Z.; Hong, X. Polymethine Thiopyrylium Fluorophores with Absorption beyond 1000 nm for Biological Imaging in the Second Near-Infrared Subwindow. *J. Med. Chem.* **2019**, *62* (4), 2049–2059.
- (24) Hu, Z.; Chen, W. H.; Tian, J.; Cheng, Z. NIRF Nanoprobes for Cancer Molecular Imaging: Approaching Clinic. *Trends Mol. Med.* **2020**, *26* (5), 469–482.

- (25) Sun, Y.; Zeng, X.; Xiao, Y.; Liu, C.; Zhu, H.; Zhou, H.; Chen, Z.; Xu, F.; Wang, J.; Zhu, M.; Wu, J.; Tian, M.; Zhang, H.; Deng, Z.; Cheng, Z.; Hong, X. Novel dual-function near-infrared II fluorescence and PET probe for tumor delineation and image-guided surgery. *Chem. Sci.* **2018**, *9* (8), 2092–2097.
- (26) Sun, Y.; Ding, M.; Zeng, X.; Xiao, Y.; Wu, H.; Zhou, H.; Ding, B.; Qu, C.; Hou, W.; Er-Bu, A.; Zhang, Y.; Cheng, Z.; Hong, X. Novel bright-emission small-molecule NIR-II fluorophores for in vivo tumor imaging and image-guided surgery. *Chem. Sci.* **2017**, *8* (5), 3489–3493.
- (27) Zhang, Z.; Cai, M.; Bao, C.; Hu, Z.; Tian, J. Endoscopic Cerenkov luminescence imaging and image-guided tumor resection on hepatocellular carcinoma-bearing mouse models. *Nanomedicine* **2019**, *17*, 62–70.
- (28) Hu, Z.; Chi, C.; Liu, M.; Guo, H.; Zhang, Z.; Zeng, C.; Ye, J.; Wang, J.; Tian, J.; Yang, W.; Xu, W. Nanoparticle-mediated radiopharmaceutical-excited fluorescence molecular imaging allows precise image-guided tumor-removal surgery. *Nanomedicine* **2017**, *13* (4), 1323–1331.
- (29) Antaris, A. L.; Chen, H.; Cheng, K.; Sun, Y.; Hong, G.; Qu, C.; Diao, S.; Deng, Z.; Hu, X.; Zhang, B.; Zhang, X.; Yaghi, O. K.; Alamparambil, Z. R.; Hong, X.; Cheng, Z.; Dai, H. A small-molecule dye for NIR-II imaging. *Nat. Mater.* **2016**, *15* (2), 235–242.
- (30) Zhang, X. D.; Wang, H.; Antaris, A. L.; Li, L.; Diao, S.; Ma, R.; Nguyen, A.; Hong, G.; Ma, Z.; Wang, J.; Zhu, S.; Castellano, J. M.; Wyss-Coray, T.; Liang, Y.; Luo, J.; Dai, H. Traumatic Brain Injury Imaging in the Second Near-Infrared Window with a Molecular Fluorophore. *Adv. Mater.* **2016**, *28* (32), 6872–6879.
- (31) Antaris, A. L.; Chen, H.; Diao, S.; Ma, Z.; Zhang, Z.; Zhu, S.; Wang, J.; Lozano, A. X.; Fan, Q.; Chew, L.; Zhu, M.; Cheng, K.; Hong, X.; Dai, H.; Cheng, Z. A high quantum yield molecule-protein complex fluorophore for near-infrared II imaging. *Nat. Commun.* **2017**, *8*, 15269.
- (32) Feng, Y.; Zhu, S.; Antaris, A. L.; Chen, H.; Xiao, Y.; Lu, X.; Jiang, L.; Diao, S.; Yu, K.; Wang, Y.; Herraiz, S.; Yue, J.; Hong, X.; Hong, G.; Cheng, Z.; Dai, H.; Hsueh, A. J. Live imaging of follicle stimulating hormone receptors in gonads and bones using near infrared II fluorophore. *Chem. Sci.* **2017**, *8* (5), 3703–3711.
- (33) Lin, J.; Zeng, X.; Xiao, Y.; Tang, L.; Nong, J.; Liu, Y.; Zhou, H.; Ding, B.; Xu, F.; Tong, H.; Deng, Z.; Hong, X. Novel near-infrared II aggregation-induced emission dots for in vivo bioimaging. *Chem. Sci.* **2019**, *10* (4), 1219–1226.
- (34) Wang, F.; Wan, H.; Ma, Z.; Zhong, Y.; Sun, Q.; Tian, Y.; Qu, L.; Du, H.; Zhang, M.; Li, L.; Ma, H.; Luo, J.; Liang, Y.; Li, W. J.; Hong, G.; Liu, L.; Dai, H. Light-sheet microscopy in the near-infrared II window. *Nat. Methods* **2019**, *16* (6), 545–552.
- (35) Hu, Z.; Fang, C.; Li, B.; Zhang, Z.; Cao, C.; Cai, M.; Su, S.; Sun, X.; Shi, X.; Li, C.; Zhou, T.; Zhang, Y.; Chi, C.; He, P.; Xia, X.; Chen, Y.; Gambhir, S. S.; Cheng, Z.; Tian, J. First-in-human liver-tumour surgery guided by multispectral fluorescence imaging in the visible and near-infrared-I/II windows. *Nat. Biomed. Eng.* **2020**, *4* (3), 259–271.
- (36) He, S.; Song, J.; Qu, J.; Cheng, Z. Crucial breakthrough of second near-infrared biological window fluorophores: design and synthesis toward multimodal imaging and theranostics. *Chem. Soc. Rev.* **2018**, *47* (12), 4258–4278.
- (37) Hong, G.; Antaris, A. L.; Dai, H. Near-infrared fluorophores for biomedical imaging. *Nat. Biomed. Eng.* **2017**, *1*, 0010.
- (38) Ding, F.; Zhan, Y.; Lu, X.; Sun, Y. Recent advances in near-infrared II fluorophores for multifunctional biomedical imaging. *Chem. Sci.* **2018**, *9* (19), 4370–4380.
- (39) Li, D.; Qu, C.; Liu, Q.; Wu, Y.; Hu, X.; Qian, K.; Chang, B.; He, S.; Yuan, Y.; Li, Y.; Ko, T.; Yu, A.; Cheng, Z. Monitoring the Real-Time Circulatory System-Related Physiological and Pathological Processes In Vivo Using a Multifunctional NIR-II Probe. *Adv. Funct. Mater.* **2020**, *30* (6), 1906343.
- (40) Benesova, M.; Bauder-Wust, U.; Schafer, M.; Klika, K. D.; Mier, W.; Haberkorn, U.; Kopka, K.; Eder, M. Linker Modification Strategies To Control the Prostate-Specific Membrane Antigen (PSMA)-Targeting and Pharmacokinetic Properties of DOTA-Conjugated PSMA Inhibitors. *J. Med. Chem.* **2016**, *59* (5), 1761–1775.
- (41) Kawatani, M.; Yamamoto, K.; Yamada, D.; Kamiya, M.; Miyakawa, J.; Miyama, Y.; Kojima, R.; Morikawa, T.; Kume, H.; Urano, Y. Fluorescence Detection of Prostate Cancer by an Activatable Fluorescence Probe for PSMA Carboxypeptidase Activity. *J. Am. Chem. Soc.* **2019**, *141* (26), 10409–10416.
- (42) Wang, X.; Huang, S. S.; Heston, W. D.; Guo, H.; Wang, B. C.; Basilion, J. P. Development of targeted near-infrared imaging agents for prostate cancer. *Mol. Cancer Ther.* **2014**, *13* (11), 2595–2606.
- (43) Chen, Y.; Chatterjee, S.; Lisok, A.; Minn, I.; Pullambhatla, M.; Wharram, B.; Wang, Y.; Jin, J.; Bhujwalla, Z. M.; Nimmagadda, S.; Mease, R. C.; Pomper, M. G. A PSMA-targeted theranostic agent for photodynamic therapy. *J. Photochem. Photobiol., B* **2017**, *167*, 111–116.
- (44) Kwon, Y. D.; Oh, J. M.; La, M. T.; Chung, H. J.; Lee, S. J.; Chun, S.; Lee, S. H.; Jeong, B. H.; Kim, H. K. Synthesis and Evaluation of Multifunctional Fluorescent Inhibitors with Synergistic Interaction of Prostate-Specific Membrane Antigen and Hypoxia for Prostate Cancer. *Bioconjugate Chem.* **2019**, *30* (1), 90–100.
- (45) Kwon, Y. D.; Chung, H. J.; Lee, S. J.; Lee, S. H.; Jeong, B. H.; Kim, H. K. Synthesis of novel multivalent fluorescent inhibitors with high affinity to prostate cancer and their biological evaluation. *Bioorg. Med. Chem. Lett.* **2018**, *28* (4), 572–576.
- (46) Shallal, H. M.; Minn, I.; Banerjee, S. R.; Lisok, A.; Mease, R. C.; Pomper, M. G. Heterobivalent agents targeting PSMA and integrin- $\alpha$ v $\beta$ 3. *Bioconjugate Chem.* **2014**, *25* (2), 393–405.
- (47) Chen, Y.; Pullambhatla, M.; Banerjee, S. R.; Byun, Y.; Stathis, M.; Rojas, C.; Slusher, B. S.; Mease, R. C.; Pomper, M. G. Synthesis and Biological Evaluation of Low Molecular Weight Fluorescent Imaging Agents for the Prostate-Specific Membrane Antigen. *Bioconjugate Chem.* **2012**, *23* (12), 2377–2385.
- (48) Duan, X.; Liu, F.; Kwon, H.; Byun, Y.; Minn, I.; Cai, X.; Zhang, J.; Pomper, M. G.; Yang, Z.; Xi, Z.; Yang, X. (S)-3-(Carboxyformamido)-2-(3-(carboxymethyl)ureido)propanoic Acid as a Novel PSMA Targeting Scaffold for Prostate Cancer Imaging. *J. Med. Chem.* **2020**, *63* (7), 3563–3576.
- (49) Staderini, M.; Martin, M. A.; Bolognesi, M. L.; Menendez, J. C. Imaging of beta-amyloid plaques by near infrared fluorescent tracers: a new frontier for chemical neuroscience. *Chem. Soc. Rev.* **2015**, *44* (7), 1807–1819.
- (50) Zhu, S.; Tian, R.; Antaris, A. L.; Chen, X.; Dai, H. Near-Infrared-II Molecular Dyes for Cancer Imaging and Surgery. *Adv. Mater.* **2019**, *31* (24), No. 1900321.
- (51) Wang, S.; Fan, Y.; Li, D.; Sun, C.; Lei, Z.; Lu, L.; Wang, T.; Zhang, F. Anti-quenching NIR-II molecular fluorophores for in vivo high-contrast imaging and pH sensing. *Nat. Commun.* **2019**, *10* (1), 1058.
- (52) Qu, C.; Xiao, Y.; Zhou, H.; Ding, B.; Li, A.; Lin, J.; Zeng, X.; Chen, H.; Qian, K.; Zhang, X.; Fang, W.; Wu, J.; Deng, Z.; Cheng, Z.; Hong, X. Quaternary Ammonium Salt Based NIR-II Probes for In Vivo Imaging. *Adv. Opt. Mater.* **2019**, *7* (15), 1900229.
- (53) Hong, G.; Robinson, J. T.; Zhang, Y.; Diao, S.; Antaris, A. L.; Wang, Q.; Dai, H. In vivo fluorescence imaging with Ag<sub>2</sub>S quantum dots in the second near-infrared region. *Angew. Chem., Int. Ed.* **2012**, *51* (39), 9818–9821.
- (54) Banerjee, S. R.; Foss, C. A.; Castanares, M.; Mease, R. C.; Byun, Y.; Fox, J. J.; Hilton, J.; Lupold, S. E.; Kozikowski, A. P.; Pomper, M. G. Synthesis and evaluation of technetium-99m- and rhenium-labeled inhibitors of the prostate-specific membrane antigen (PSMA). *J. Med. Chem.* **2008**, *51* (15), 4504–4517.
- (55) Rais, R.; Rojas, C.; Wozniak, K.; Wu, Y.; Zhao, M.; Tsukamoto, T.; Rudek, M. A.; Slusher, B. S. Bioanalytical method for evaluating the pharmacokinetics of the GCP-II inhibitor 2-phosphonomethyl pentanedioic acid (2-PMPA). *J. Pharm. Biomed. Anal.* **2014**, *88*, 162–169.